

Electronic and magnetic properties of single-layer and double-layer VX2 (X = Cl, Br) under biaxial stress_

Xing Li(李兴), Yanfeng Ge(盖彦峰), Jun Li(李军), Wenhui Wan(万文辉), and Yong Liu(刘永)

Citation: Chin. Phys. B, 2021, 30 (**10**): 107305. DOI: 10.1088/1674-1056/ac0906
Journal homepage: http://cpb.iphy.ac.cn; http://iopscience.iop.org/cpb

What follows is a list of articles you may be interested in

High-resolution angle-resolved photoemission study of large magnetoresistance topological semimetal $CaAl_4$

Xu-Chuan Wu(吴徐传), Shen Xu(徐升), Jian-Feng Zhang(张建丰), Huan Ma(马欢), Kai Liu(刘凯), Tian-Long Xia(夏天龙), and Shan-Cai Wang(王善才)

Chin. Phys. B, 2021, 30 (**9**): 097303. DOI: 10.1088/1674-1056/ac0cd7

First-principles study of plasmons in doped graphene nanostructures

Xiao-Qin Shu(舒晓琴), Xin-Lu Cheng(程新路), Tong Liu(刘彤), and Hong Zhang(张红)

Chin. Phys. B, 2021, 30 (**9**): 097301. DOI: 10.1088/1674-1056/abe92d

Giant Rashba-like spin-orbit splitting with distinct spin texture in two-dimensional heterostructures

Jianbao Zhu(朱健保), Wei Qin(秦维), and Wenguang Zhu(朱文光)

Chin. Phys. B, 2021, 30 (**8**): 087307. DOI: 10.1088/1674-1056/ac0784

Fabrication of sulfur-doped cove-edged graphene nanoribbons on Au(111)

Huan Yang(杨欢), Yixuan Gao(高艺璇), Wenhui Niu(牛雯慧), Xiao Chang(常霄), Li Huang(黄立), Junzhi Liu(刘俊治), Yiyong Mai(麦亦勇), Xinliang Feng(冯新亮), Shixuan Du(杜世萱), and Hong-Jun Gao(高鸿钧)

Chin. Phys. B, 2021, 30 (**7**): 077306. DOI: 10.1088/1674-1056/abfbd0

Quantization of the band at the surface of charge density wave material 2H-$TaSe_2$

Man Li(李满), Nan Xu(徐楠), Jianfeng Zhang(张建丰), Rui Lou(娄睿), Ming Shi(史明), Lijun Li(黎丽君), Hechang Lei(雷和畅), Cedomir Petrovic, Zhonghao Liu(刘中灏), Kai Liu(刘凯), Yaobo Huang(黄耀波), and Shancai Wang(王善才)

Chin. Phys. B, 2021, 30 (**4**): 047305. DOI: 10.1088/1674-1056/abe9a8

Electronic and magnetic properties of single-layer and double-layer VX_2 (X = Cl, Br) under biaxial stress*

Xing Li(李兴), Yanfeng Ge(盖彦峰), Jun Li(李军), Wenhui Wan(万文辉), and Yong Liu(刘永)†

State Key Laboratory of Metastable Materials Science and Technology & Key Laboratory for Microstructural Material Physics of Hebei Province, School of Science, Yanshan University, Qinhuangdao 066004, China

(Received 2 April 2021; revised manuscript received 31 May 2021; accepted manuscript online 8 June 2021)

First-principles calculations and Monte Carlo simulations reveal that single-layer and double-layer VX_2 (X = Cl, Br) can be tuned from antiferromagnetic (AFM) semiconductors to ferromagnetic (FM) state when biaxial tensile stress is applied. Their ground states are all T phase. The biaxial tensile stress at the phase transition point of the double-layer VX_2 is larger than that of the single-layer VX_2. The direct band gaps can be also manipulated by biaxial tensile stress as they increases with increasing tensile stress to a critical point and then decreases. The Néel temperature (T_N) of double-layer VX_2 are higher than that of single-layer. As the stress increases, the T_N of all materials tend to increase. The magnetic moment increases with the increase of biaxial tensile stress, and which become insensitive to stress after the phase transition points. Our research provides a method to control the electronic and magnetic properties of VX_2 by stress, and the single-layer and double-layer VX_2 may have potential applications in nano spintronic devices.

Keywords: first-principles, biaxial tensile stress, phase transition, magnetic properties

PACS: 73.22.−f, 31.15.A−, 64.60.−i **DOI:** 10.1088/1674-1056/ac0906

1. Introduction

Since graphene[1] with weak interlayer van der Waals (vdW) interaction was successfully exfoliated, two-dimensional (2D) materials have received extensive attention from scientists. Many 2D materials with excellent optical,[2,3] mechanical,[4] electrical,[5–7] and magnetic[8,9] properties have been widely studied, such as: phosphorene,[10,11] transition metal dichalcogenides (TMDs),[12,13] and CrI_3.[14–16] Among them, 2D magnetic semiconductor materials have great potential in spintronic devices[17,18] due to their magnetic properties and ultra-thin thickness.

The large area and outstanding stretchability of 2D materials allow its magnetic properties be tailored by external field. For example, when an external electric field[19] is applied to this CrI_3, electrons transporting through the CrI_3 barriers will generate huge magnetoresistance[15,16,20] due to the spin filtering effect. Song *et al.* proposed that the perpendicular electric field can adjust the splitting energy and reverse the spin splitting direction in the vdW monolayer arsenene/$FeCl_2$ heterostructures.[21] On the other side, stress engineering is also a common method to control the magnetic properties of 2D materials. The stress on the 2D material can be realized by the methods of substrate effect[22–24] and piezoelectric actuators[25,26] in the experiments. Zhu *et al.* pointed that the magnetic anisotropy energy of the 2D vdW GeS/$FeCl_2$ multiferroic heterostructures can be increased by applying biaxial compressive strain.[27] Zhang *et al.* found that there is a strain-induced phase transition from half semiconductor to bipolar magnetic semiconductor in the Janus $Cr_2I_3X_3$ (X = Cl, Br) monolayer.[28] When a biaxial tensile stress of 3.5% is applied to the single-layer of MoS_2 doped with single Fe atom, its magnetic moment changes from 2.04 μ_B to 4 μ_B.[12] Besides, there are phase transitions between the FM state and the AFM state in 2D materials[29–31] when stress is applied. For instance, when a biaxial compressive stress is applied, single layer CrI_3[29] has a phase transition from FM state to AFM state, and single layer $MnPSe_3$[30] has a phase transition from AFM state to FM state.

Inspired by the research of 2D material under external stress field, we put the research goal on 2D transition metal dihalides VX_2 (X = Cl, Br). There are three stable phases[13,32–34] (T phase, H phase, and T_d phase) in the widely studied 2D TMDs.[35,36] Since 2D transition metal dihalides and TMDs differ only in non-metallic atoms, we also use the phases mentioned above to analyze 2D transition metal dihalide VX_2. Several theoretical works[37,38] have displayed that the ground state of free-standing single-layer VX_2 in both 1H and 1T phases are AFM. In this work, we systematically investigated the mechanical, dynamic, electronic, and magnetic properties of single-layer and double-layer VX_2 under different stresses. Similar to previous work,[39] different stacking patterns are considered in constructing double-layer VX_2. We find that the ground states of the single and double layer VX_2 are AFM semiconductors with T phase, and they are

*Project supported by the National Natural Science Foundation of China (Grant Nos. 11904312 and 11904313), the Project of Hebei Educational Department, China (Grant Nos. ZD2018015 and QN2018012), and the Natural Science Foundation of Hebei Province, China (Grant No. A2019203507).

†Corresponding author. E-mail: yongliu@ysu.edu.cn

© 2021 Chinese Physical Society and IOP Publishing Ltd

mechanically and kinetically stable. A phase transition from AFM state to FM state occurs when the biaxial tensile stress is applied. The mechanism of the magnetical phase transition is the competition between direct exchange and superexchange interactions. The band gaps increase and then turn to decreasing under biaxial tensile stress. Besides, applying stress to the VX_2 can increase the value of T_N.

2. Theoretical method

In the framework of density functional theory (DFT), the electronic structure and magnetic properties of materials were studied using the projector augmented wave (PAW) method, which was implemented in the Vienna *ab initio* simulation software package (VASP).[40,41] Perdew–Burke–Ernzerhof (PBE) was used to process the exchange relation function.[42] In this paper, a supercell size of $2\times2\times1$ unit cells was used to study the magnetic structures in the calculations. A cutoff energy of 600 eV and a Γ-centered Monkhorst–Pack k-points mesh of $9\times9\times1$ for the Brillouin zone was found to be sufficient to obtain the convergence. The conjugate-gradient algorithm was employed for geometry optimization using convergence criterion of 10^{-6} eV for the total energy and 0.01 eV/Å for Hellmann–Feynman force components. Using the density functional perturbation theory (DFPT)[43] to calculate the phonon spectrum, the convergence criterion of 10^{-10} eV for the total energy and 10^{-5} eV/Å for Hellmann–Feynman force components. We included the vdW correction in all the calculations using zero damping DFT-D3 method of Grimme.[44]

3. Results and discussion

The present work explores single-layer and double-layer VX_2 (X = Cl, Br) with the three most common phases in TMDs, namely T, H, and T_d phases.[13,32,34] Since the single-layer and double-layer materials can be constructed by peeling off one or two layers from bulk materials, we need to construct the bulk structures at first. For the single-layer T-phase structure, there are three unequal positions (named A, B, C) in the c-axis direction, which are the position of one V atom and the positions of two X atoms. And the single-layer H-phase structure has two unequal positions (named A, B) in the c-axis direction. Therefore, we could consider different stackings for the bulk structures. For example, AA stacking, AB stacking, and ABC stacking (stacking here only considers the different stacking methods of V atoms) are shown in Fig. 1 and Figs. A1–A3 in Appendix A: Supplemental material (See supplemental material for more details on the structures constructed, antiferromagnetic configurations of single-layer structure, phonon spectrums, the formula for calculating the exchange correlation constant of double layer materials, and the exchange correlation constant of the ground-state single-layer and double-layer VX_2). The bulk T-phase structure (ABC stacking) has hexagonal lattice, which belongs to the $R\bar{3}m$ space group (166). In calculations, the non-magnetic (NM), FM, and AFM states are considered, by optimizing the atomic position and lattice constant to find the lowest energy states. The structures of T_d phase and T′ phase would turn to the corresponding stacking forms of T phase when magnetism is considered, and the only difference between T_d-phase and T′-phase structures is the stacking. In the following calculations, we only consider the T-phase and H-phase structures.

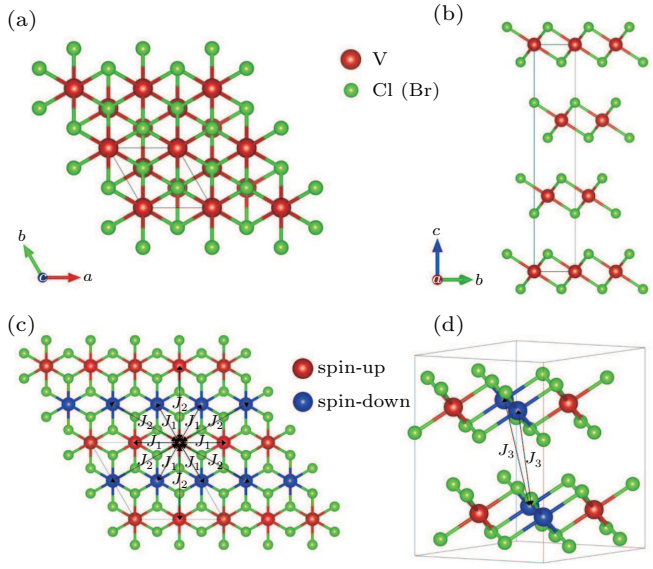


Fig. 1. The schematic diagrams of the ground-state structure of the bulk transition metal dihalide VX_2 (X = Cl, Br) in the c direction (a) and a direction (b). The ground-state AFM configurations of single-layer (c) and double-layer (d) transition metal dihalide VX_2 (X = Cl, Br), respectively. J_1 and J_2 represent the exchange correlation constant of the nearest neighbor and next-nearest neighbor in the layer, and J_3 represents the exchange correlation constant of the third nearest neighbor between the layers.

The cleavage energy is the energy required to cleave the bulk materials in two halves,[45] which is a criterion for judging whether the bulk material is easy to peel off. The formula used to calculate the cleavage energy gives $E_c = E_s - E_t$, where E_s denotes the total energy of two separate parts and E_t denotes the total energy of the bulk. We find that the cleavage energy (see Table 1) of all structures considered in the article are less than that of graphene[46] (0.36 J/m^2), so they are easy to be peel off. Furthermore, the formation energy determine the difficulty for sythesision of VX_2. For the binary compound VX_2, the expression for the formation energy can be written as

$$E_f = \frac{E(VX_2) - E(V) - 2E(X)}{3}, \tag{1}$$

where $E(V)$, $E(X)$, and $E(VX_2)$ are the normalized energy of the stable bulk bcc-V, gas phases (Cl_2, Br_2), and bulk VX_2, respectively. See Table 1, since the formation energies of all stuctures considered in this paper have negative values, which are experimentally stable.

Table 1. A summary table of the formation and cleavage energy of bulk VCl_2 and VBr_2. E_c stands for cleavage energy and E_f stands for formation energy.

VCl_2			VBr_2		
Phase	E_f (eV/atom)	E_c (J/m^2)	Phase	E_f (eV/atom)	E_c (J/m^2)
T_{AA}	−1.323	0.301	T_{AA}	−1.042	0.306
T_{ABC}	−1.324	0.257	T_{ABC}	−1.043	0.277
T_{AB}	−1.324	0.280	T_{AB}	−1.043	0.284
H_{AA}	−1.106	0.242	H_{AA}	−0.815	0.212
H_{AB}	−1.118	0.299	H_{AB}	−0.832	0.311

In order to determine the most stable phases in all structures, one NM, one FM, and four AFM configurations are considered for the single-layer structure. For the double-layer structure, one NM, one FM, and seven AFM configurations[47] are considered. We find that the T-phase of the single-layer structure has lower formation energies, and the ground state magnetic order (named AFM2) is shown in Fig. 1(c) which is consistent with previous work.[37,38] The ABC stacking double-layer structure with T phase is more stable, and the ground-state AFM configuration is shown in Fig. 1(d). In Table 2, the NM state has higher energy than the magnetic state, only the corresponding AFM configuration of the ground state is considered in the following calculations. Furthermore, in order to test the dynamic stability of the ground state single-layer and double-layer structures, we provide the corresponding phonon spectrums in Fig. A5. There is no imaginary frequencies, implying the kinetic stability of the single-layer and double-layer VX_2.

Figure 2 shows the electronic band structures and project density of states (PDOS) of the ground-state phases (the structure shown in Fig. 1). The indirect band gaps of the double-layer VX_2 (1.0276 eV for X = Cl, 1.0170 eV for X = Br) is smaller than that of the single-layer VX_2 (1.0713 eV for X = Cl, 1.0472 eV for X = Br). Further, the electronic band structure of the double-layer structure is different from that of the single-layer structure in the K to Γ range. The electrons of the d orbital of the V atom that play a major role to the band structure in this range. Due to the coupling between the layers, the electrons are not only localized in the plane, but also a small amount of electrons in a small range close to the plane, which leads to the difference in the band structure between K and Γ. The density of states (DOS) of all materials near the Fermi energy is reduced to zero, make these materials semi-conductivity.

Table 2. The normalized energy table of the ground state (AFM state), FM state, and NM state of single-layer and double-layer VX_2 (X = Cl, Br). s-T represents single-layer T-phase structure, and d-T represents double-layer T-phase structure.

VCl_2				VBr_2			
Structure	AFM	FM	NM	Structure	AFM	FM	NM
s-T (eV)	−16.062	15.993	−15.323	s-T (eV)	−14.716	−14.678	-13.784
d-T (eV)	−16.483	−16.400	−15.804	d-T (eV)	−15.228	−15.179	−14.368

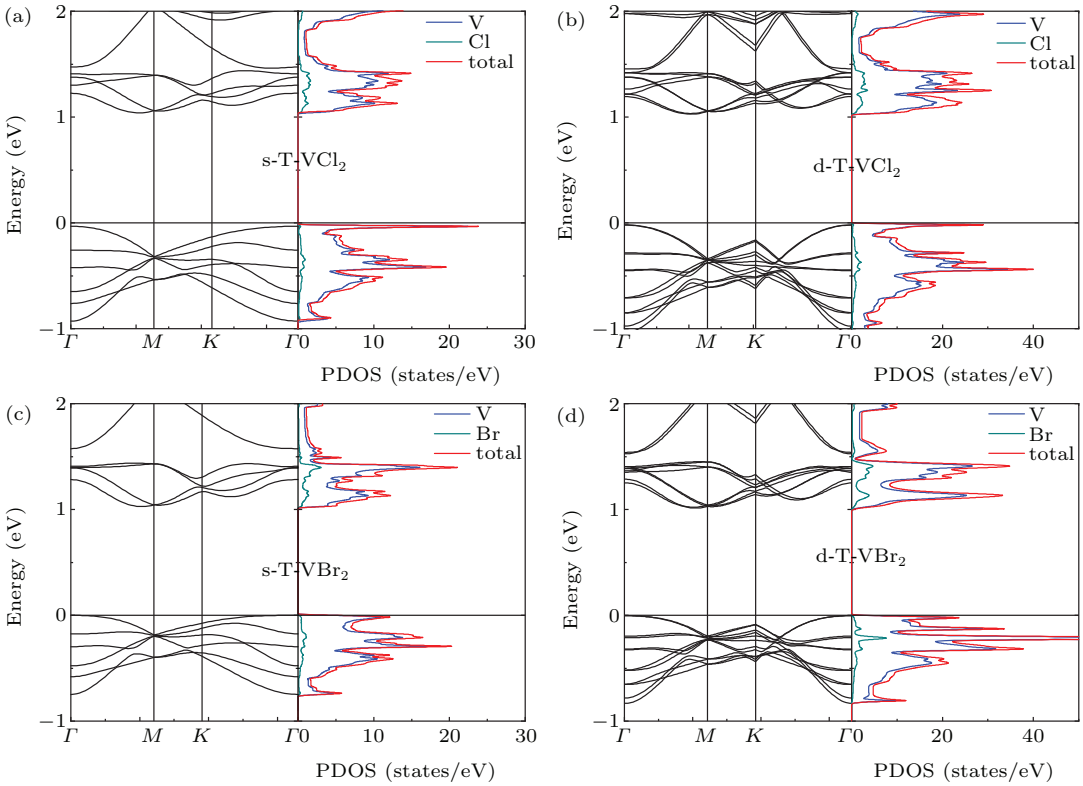


Fig. 2. The ground-state electronic band structures and project density of states (PDOS) of (a) s-T-VCl_2, (b) d-T-VCl_2, (c) s-T-VBr_2, and (d) d-T-VBr_2.

For the 2D material VX_2 (X = Cl, Br), the microscopic mechanisms of VX_2, which determine the magnetic properties, contain two parts: (i) direct AFM exchange interaction between two V atoms; (ii) FM superexchange interaction among V–Cl (Br)–V with an anionic mediation Cl (Br). The competition between AFM and FM may lead to different magnetic ground state. When the direct exchange interaction between two V atoms is stronger than the superexchange interaction between V–Cl (Br)–V, the ground state of the material shows AFM, otherwise it is FM. Here, the direct exchange interaction between V atoms is dominant in these systems. For AFM materials, the Néel temperature (T_N)[48,49] refers to a parameter of the temperature at which the AFM phase of the antiparallel magnetic order changes to the NM phase. We use the Ising model in the Monte Carlo method to calculate it. The Hamiltonian[50] can be written in the following form:

$$H = -\sum_{\langle ij \rangle} J_{ij} S_i S_j, \tag{2}$$

where J_{ij} represents the exchange interactions of over all neighbor V–V pairs, S_i represents the spin of the atom i. For the single-layer structure, this paper considers the nearest neighbor and the next nearest neighbor interaction, and the third nearest neighbor interaction between the layers is also considered for the double-layer structure. To calculate J, we write the energy of the single-layer VX_2 in the FM, AFM2, and AFM4 configurations (shown in Fig. A4) in the following form:

$$E_{FM} = E_0 - 6J_1S^2 - 6J_2S^2, \tag{3}$$

$$E_{AFM2} = E_0 + 2J_1S^2 + 2J_2S^2, \tag{4}$$

$$E_{AFM4} = E_0 + 2J_1S^2 - 2J_2S^2, \tag{5}$$

where J_1 and J_2 (shown in Fig. 1(c)) represent the exchange correlation constant of the nearest neighbor and the next nearest neighbor, and E_0 is the energy of a single-layer VX_2 without spin polarization and $S = 3/2$.[51] Through calculations, the absolute value of J_1 for all materials is much greater than J_2 (J_3), and the value of J_1 is negative (in the Table A1), which further verifies the antiferromagnetism of the ground states. We use the Metropolis algorithm and a 32×32 2D supercell with periodic boundary conditions to compute T_N, and the calculations are implemented in mcsolver software.[52] Besides, because 2D materials have excellent stretchability, the pressure factor is also taken into account in the calculations. Figure 3 shows that the Monte Carlo simulations of T_N of the single-layer and double-layer VX_2 with pressure. When no stress is applied, the T_N of single-layer and double-layer VCl_2 is 62 K and 96 K, and the value of single-layer and double-layer VBr_2 is 32 K and 144 K. Compared with the single-layer VX_2, the T_N of the double-layer VX_2 are higher. In Table 2, the normalized energy of the double-layer structure is lower than that of the single-layer structure, so the coupling effect between the layers makes the double-layer systems more stable and higher T_N. When stress is applied to the materials, as the stress increases, the T_N of all materials tend to increase.

Further, we calculate the Curie temperature (T_c) of the ferromagnetic state under a tensile stress of 8%, the T_c of single-layer and double-layer VCl_2 is 53 K and 24 K, respectively. Due to the 8% stress is close to the phase transition point of single-layer and double-layer VCl_2, the small exchange correlation constant results in a low Curie temperature. The T_c of single-layer and double-layer VBr_2 is 175 K and 293 K, respectively. The latter one is close to the room temperature.

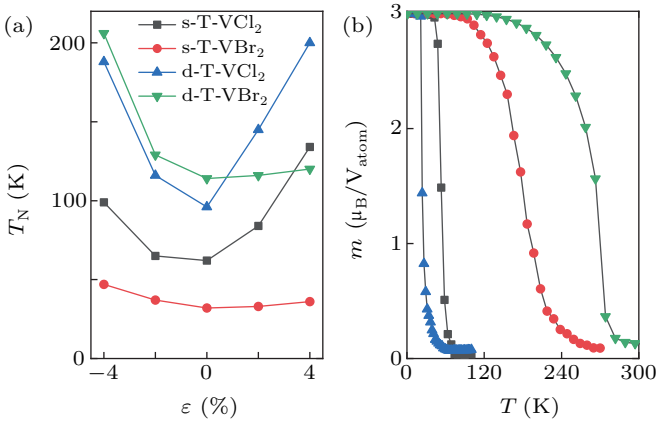


Fig. 3. (a) The Néel temperature of single-layer and double-layer VCl_2 and VBr_2 under stress. (b) The Curie temperature of single-layer and double-layer VCl_2 and VBr_2 under 8% biaxial tensile stress, m represents the total magnetic moment per V atom.

We also explore the magnetic state, magnetic moment and band gap depends of biaxial stress. From Fig. 4(a), the ground states of all materials change from an AFM state to an FM state when the biaxial tensile stress reaches the corresponding critical point. Meanwhile, there are no phase transitions under biaxial compressive stress. The stress of the phase transition points of the single-layer and double-layer VCl_2 are 6.65% and 7.64%, while the single-layer and double-layer VBr_2 are 4.49% and 5.32%. For the same material, the phase transition stress for a double-layer structure is greater than that of a single-layer structure. See Fig. 4(b), the band gaps also changes under by applying biaxial stress. When applying pressure, the band gaps of all materials gradually decrease. However, when stress increases, the band gaps of all materials firstly become larger and then turn smaller. Noted that the band gaps decrease rapidly near the phase transition point. In Fig. 4(c), we find that the magnetic moment gradually decreases and increases under biaxial compressive and tensile stress, respectively. As the spin-polarized charges of VX_2 (X = Cl and Br) mainly arise from the localized nonbonding V-3d electrons, the increase of tensile stress reduces the covalent interaction between V and Cl or Br atoms. As a result, the number of nonbonding V-3d electrons increases, so that the magnetic moment of V atomic increases.[53] On the other side, compressive stress has the opposite effect. Moreover, the

magnetic moment jumps at the phase transition points, and becomes insensitive to stress after the phase transition points.

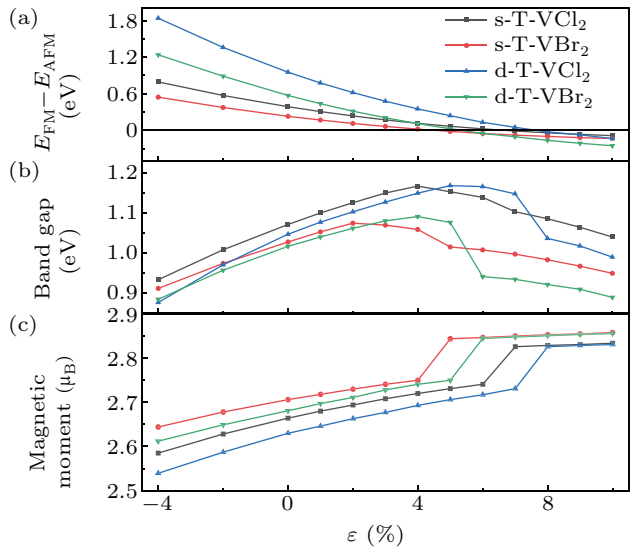


Fig. 4. (a) Magnetic ground state, (b) band gap, and (c) magnetic moment of single-layer and double-layer VCl_2 and VBr_2 under biaxial stress.

4. Conclusion

In summary, we explore the ground state phases among the possible structures of single-layer and double-layer VX_2 (X = Cl, Br) based on first-principles calculations. The electronic and magnetic properties of the corresponding phase under biaxial stress are systematically investigated. The ground states of single-layer and double-layer VX_2 are all AFM semiconductors with T phase, and are dynamically and mechanically stable. All ground-state structures only have one phase transition from AFM to FM under biaxial tensile stress. The mechanism of the magnetic phase transition is the competition between direct exchange and superexchange interactions. The band gaps increase and then turn to decreasing under biaxial tensile stress. T_N of the single-layer are lower than that of double-layer VX_2 according to Monte Carlo simulations, which may be caused by the coupling effect between the layers. Besides, applying stress to the VX_2 can increase the value of T_N and the magnetic moment increases as the biaxial tensile stress increases. In 2015, Lv *et al.*[54] summarized controlled synthesis of 2D TMDs using wet chemical approaches, chemical exfoliation, and chemical vapor deposition (CVD). Meanwhile, it is possible to control the number of layers when synthesizing these materials. Our results show that single-layer and double-layer VX_2 (X = Cl, Br) would possess potential applications in spintronic devices. We also hope that our theoretical research will be helpful to the further experiment.

Acknowledgment

Thanks to the teachers and classmates who have helped me, and thanks to my parents and friends for their supports.

Appendix A: Supplemental material

In order to better understand and explain the descriptions in the main text, some figures, formulas, and table are given below.

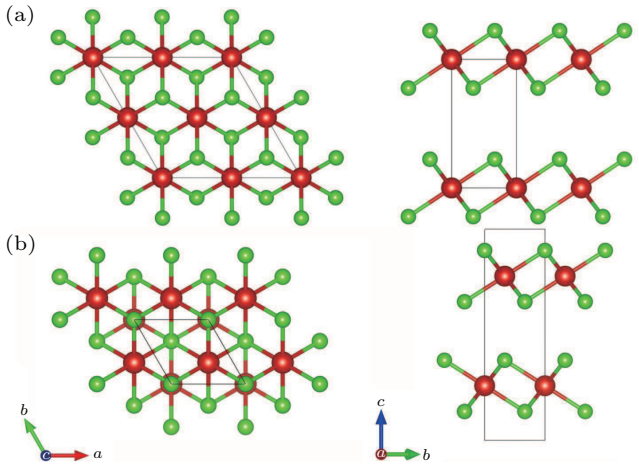


Fig. A1. The schematic diagrams of the bulk T-phase VX_2 (X = Cl, Br) of (a) AA stacking and (b) AB stacking.

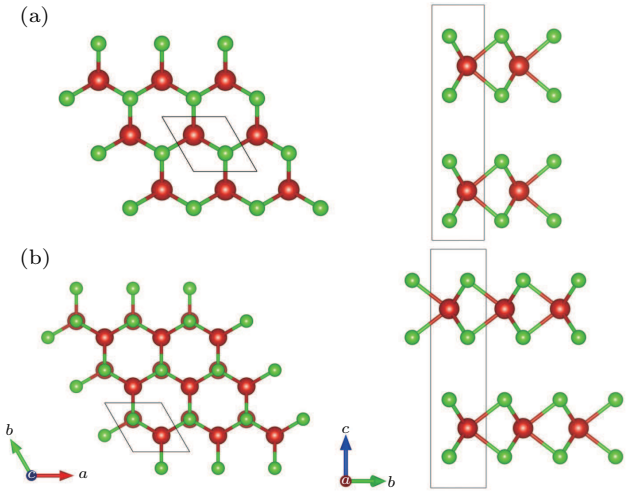


Fig. A2. The schematic diagrams of the bulk H-phase VX_2 (X = Cl, Br) of (a) AA stacking and (b) AB stacking.

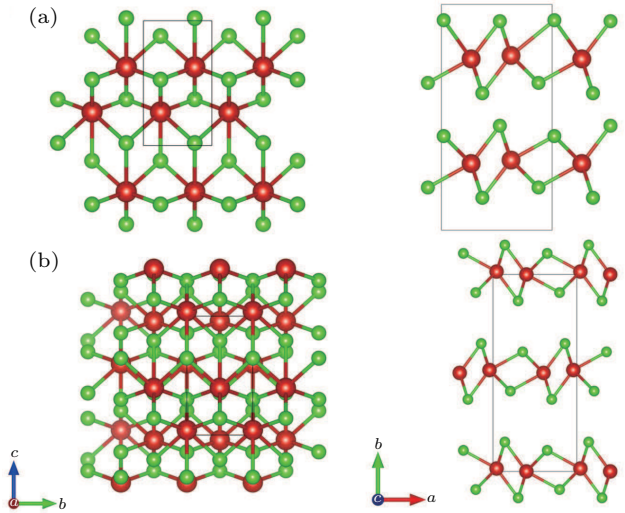


Fig. A3. The schematic diagrams of the bulk VX_2 (X = Cl, Br) of (a) T′-phase and (b) T_d-phase.

Table A1. The exchange correlation constants of the ground-state single-layer and double-layer VX_2.

Structure	s-T-VCl_2	s-T-VBr_2	d-T-VCl_2	d-T-VBr_2
J_1 (meV)	−3.7586	−2.1451	−9.1791	−5.3553
J_2 (meV)	−0.0885	−0.0077	−0.0466	−0.1612
J_3 (meV)	–	–	0.0776	0.0415

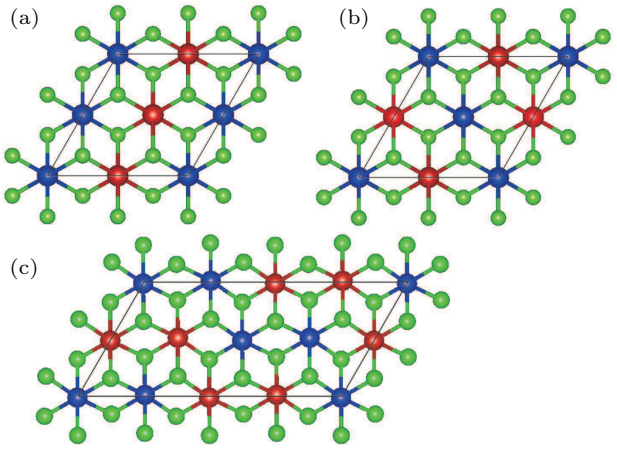


Fig. A4. The antiferromagnetic configurations of single-layer VX_2 of (a) AFM1, (b) AFM3, and (c) AFM4.

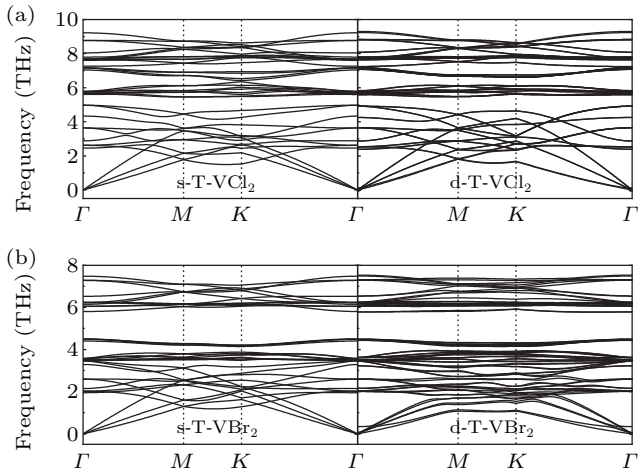


Fig. A5. Phonon spectrum of the ground-state single-layer and double-layer (a) VCl_2 and (b) VBr_2.

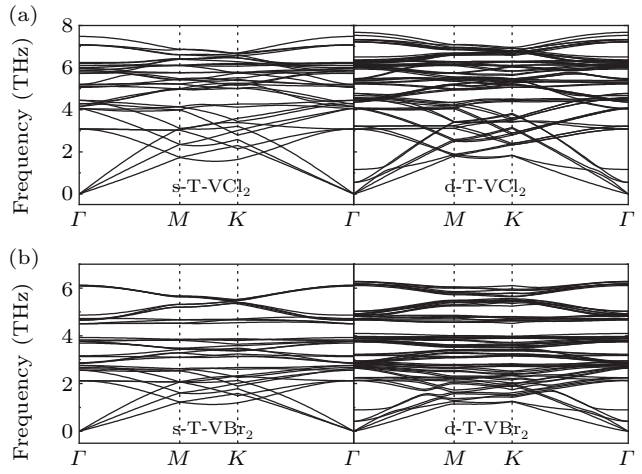


Fig. A6. Phonon spectrum of the ground-state single-layer and double-layer (a) VCl_2 and (b) VBr_2 under 10% tensile stress.

The formulas for calculating the exchange correlation constants of double layer materials are given below:

$$E_{\mathrm{FM}} = E_0 - 6J_1S^2 - 6J_2S^2 - 2J_3S^2, \tag{A1}$$

$$E_{\mathrm{A\text{-}AFM}} = E_0 - 6J_1S^2 - 6J_2S^2 + 2J_3S^2, \tag{A2}$$

$$E_{\mathrm{C\text{-}AFM}} = E_0 + 2J_1S^2 + 2J_2S^2 - 2J_3S^2, \tag{A3}$$

$$E_{\mathrm{A^*\text{-}AFM}} = E_0 + 2J_1S^2 + 2J_2S^2 - 2J_3S^2. \tag{A4}$$

References

[1] Castro Neto A H, Guinea F, Peres N M R, Novoselov K S and Geim A K 2009 *Rev. Mod. Phys.* **81** 109
[2] Mak K F, Lee C, Hone J, Shan J and Heinz T F 2010 *Phys. Rev. Lett.* **105** 136805
[3] Splendiani A, Sun L, Zhang Y, Li T and Kim J 2010 *Nano Lett.* **10** 1271
[4] Zhao H, Min K and Aluru N R 2009 *Nano Lett.* **9** 3012
[5] Booth T, Geim A K, Jiang D, Khotkevich V V, Morozov S M and Novoselov K S 2005 *Proc. Natl. Acad. Sci. USA* **102** 10451
[6] Zhang Y, Tan Y W, Stormer H L and Kim P 2005 *Nature* **438** 201
[7] Radisavljevic B, Radenovic A, Brivio J, Giacometti V and Kis A 2011 *Nat. Nanotechnol.* **6** 147
[8] Ueda K, Tabata H and Kawai T 2001 *Appl. Phys. Lett.* **79** 988
[9] Khazaei M, Arai M, Sasaki T, Chung C Y, Venkataramanan N S, Estili M, Sakka Y and Kawazoe Y 2013 *Adv. Funct. Mater.* **23** 2185
[10] Miró P, Audiffred M and Heine T 2014 *Chem. Soc. Rev.* **43** 6537
[11] Liu H, Neal A T, Zhu Z, Luo Z, Xu X, Tománek D and Ye P D 2014 *ACS Nano* **8** 4033
[12] Chen Z, He J, Zhou P, Na J and Sun L 2015 *Comp. Mater. Sci.* **110** 102
[13] Bastos C M O, Besse R, Silva J L F D and Sipahi G M 2019 *Phys. Rev. Mater.* **3** 044002
[14] Huang B, Clark G, Navarro-Moratalla E, Klein D R, Cheng R, Seyler K L, Zhong D, Schmidgall E, Mcguire M A and Cobden D H 2017 *Nature* **546** 270
[15] Song T, Cai X, Tu W Y, Zhang X, Huang B, Wilson N P, Seyler K L, Zhu L, Taniguchi T and Watanabe K 2018 *Science* **360** 1214
[16] Wang Z, Ignacio G L, Nicolas U, Martin K, Marco G, Takashi T, Kenji W, Ata I, Enrico G and Morpurgo A F 2018 *Nat. Commun.* **9** 2516
[17] Hirohata A and Takanashi K 2014 *J. Phys. D: Appl. Phys.* **47**, 193001
[18] Candini A, Klyatskaya S, Ruben M, Wernsdorfer W and Affronte M 2011 *Nano Lett.* **11** 2634
[19] Jiang S, Shan J and Mak K F 2018 *Nat. Mater.* **17** 406
[20] Song T, Tu W Y, Carnahan C, Cai X and Xu X 2019 *Nano Lett.* **19** 915
[21] Song Y, Li D, Mi W, Wang X and Cheng Y 2016 *J. Phys. Chem. C* **120** 5618
[22] Rieger W, Metzger T, Angerer H, Dimitrov R, Ambacher O and Stutzmann M 1996 *Appl. Phys. Lett.* **68** 970
[23] Wan K 2006 *Appl. Phys. Lett.* **88** 251910
[24] Frisenda R, Drüppel M, Schmidt R, Michaelis de Vasconcellos S, Perez de Lara D, Bratschitsch R, Rohlfing M and Castellanos-Gomez A 2017 *Npj 2D Mater. Appl.* **1** 10
[25] Ding F, Ji H, Chen Y, Herklotz A, Dörr K, Mei Y, Rastelli A and Schmidt O G 2010 *Nano Lett.* **10** 3453
[26] Romanov A E, Baker T J, Nakamura S and Speck J S 2006 *J. Appl. Phys.* **100** 023522
[27] Zhu Y, Wang X and Mi W 2019 *J. Mater. Chem. C* **7** 2049
[28] Zhang F, Mi W and Wang X 2020 *Adv. Electron. Mater.* **6** 1900778
[29] Wang H, Eyert V and Schwingenschlgl U 2011 *J. Phys.: Condens. Mat.* **23** 116003
[30] Pei Q, Wang X C, Zou J J and Mi W B 2018 *Front. Phys.* **013** 137105
[31] Hu T, Wan W, Ge Y and Liu Y 2020 *J. Magn. Magn. Mater.* **497** 165941
[32] Voiry D, Mohite A and Chhowalla M 2015 *Chem. Soc. Rev.* **44** 2702
[33] Hulliger F 1976 *Structural Chemistry of Layer-Type Phases* (Netherlands: Lévy F) pp. 3–39
[34] Yang H, Kim S W, Chhowalla M and Lee Y H 2015 *Nat. Phys.* **13** 931937
[35] Deng K, Wan G, Deng P, Zhang K, Ding S, Wang E, Yan M, Huang H, Zhang H and Xu Z 2016 *Nat. Phys.* **12** 1105

[36] Pen L, Yuan Y, Li G, Yang X, Xian J J, Yi C J, Shi Y G and Fu Y S 2017 *Nat. Commun.* **8** 659
[37] Feng Y, Wu X, Han J and Gao G 2018 *J. Mater. Chem. C* **6** 4087
[38] Vadym V K and Wei H 2017 *J. Mater. Chem. C* **5** 8734
[39] Zhang F, Zhang H, Mi W and Wang X 2020 *Phys. Chem. Chem. Phys.* **22** 8647
[40] Blöchl P E 1994 *Phys. Rev. B* **50** 17953
[41] Kresse G and Furthmüller J 1996 *Phys. Rev. B* **54** 11169
[42] Ernzerhof M and Scuseria G E 1999 *J. Chem. Phys.* **110** 5029
[43] Baroni S, Gironcoli S D, Corso A D and Giannozzi P 2001 *Rev. Mod. Phys.* **73** 515
[44] Grimme S, Antony J, Ehrlich S and Krieg S 2010 *J. Comput. Chem.* **27** 1787
[45] Björkman T, Gulans A, Krasheninnikov A V and Nieminen R M 2012 *Phys. Rev. Lett.* **108** 235502
[46] Joe M, Lee H, Alyrk M M, Lee J, Kim S Y, Lee C and Lee J H 2017 *J. Phys.: Condens. Matter* **29** 405801
[47] Siberchicot B, Jobic S, Carteaux V, Gressier P and Ouvrard G 1996 *J. Chem. Phys.* **100** 5863
[48] Yasuda C, Todo S, Hukushima K, Alet F, Keller M, Troyer M and Takayama H 2005 *Phys. Rev. Lett.* **94** 217201
[49] Morin F J 1959 *Phys. Rev. Lett.* **3** 34
[50] Dirac P A M 1950 *Can. J. Math.* **2** 129148
[51] Botana A S and Norman M R 2019 *Phys. Rev. Mater.* **3** 044001
[52] Liu L, Ren X, Xie J, Cheng B, Liu W, An T, Qin H and Hu J 2019 *Appl. Surf. Sci.* **480** 300
[53] Zhou Y, Su Q, Wang Z, Deng H and Zu X 2013 *Phys. Chem. Chem. Phys.* **15** 18464
[54] Lv R, Robinson J A, Schaak R E, Sun D, Sun Y, Mallouk T E and Terrones M 2015 *Acc. Chem. Res.* **48** 56